Application of a microstrain continuum to size effects in bending and torsion of foams

Article published in International Journal of Engineering Science, 101(2016), 81–91. The final publication is available at www.sciencedirect.com, doi:10.1016/j.ijengsci.2015.12.006

Geralf Hütter

Abstract

Classical theories of bending and torsion predict that the stiffness of a specimens scales with the square of the cross sectional area. However, many experiments have shown that this relation does not hold if the dimensions of the cross section become comparable to relevant length scales of the microstructure. In particular, such size effects are significant for foam materials which are nowadays extensively used in lightweight applications, since the cell size as relevant microstructural length may often be in the range of the structural component. In a number of studies, Cosserat theory was used phenomenologically to capture size effects of foam materials. However, this theory cannot describe all observed size effects and the determination of the increased number of parameters is not trivial. Recently, a model for foam materials was derived from a strict homogenisation within the microstrain framework.

The scope of the present study is to investigate whether this microstrain model is suitable to describe the size effects of foams. For this purpose, the analytical solutions for elastic torsion and bending are derived for the microstrain theory. A comparison with experimental data from literature demonstrates that the model can adequately describe the size effects in bending and torsion of closed-cell polymeric foams. Only for very high porosities the size effects are overestimated.

Keywords: size effects, micromorphic theory, closed-cell foams, bending, torsion

1 Introduction

Classical theory of continuum mechanics rests on the assumption that representative volume elements are deforming homogeneously over the microstructure, i.e. that the wave lengths of macroscopic deformation fields are much larger than the relevant length scales of the microstructure. Correspondingly, the results of experiments violating this conditions (either real or numerical ones) exhibit deviations from the predictions of classical continuum theories. For instance, strength and stiffness become dependent on the size of the employed specimens if the latter becomes comparable to the relevant microstructural length scale. In general, such deviations from predictions of classical theories are referred to as *size-effects*. Which length scale is the relevant one depends strongly on the material and active mechanisms. Whereas in brittle single crystals, the atomic lattice parameters form this length scale, thus lying in the sub-nanometer regime, grain size and mean distance of dislocations, both in the range of micrometers, are relevant for the plastic deformation behavior of typical engineering metals (e. g. [14]).

In contrast, in foams, which are applied nowadays in light-weight constructions, the cell size forms a relevant length which may lie in the range of up to millimeters. The cell size is thus comparable to typical dimensions of components giving rise to size effects, e. g. under bending as sketched in Figure 1a. Due to the relevance in light-weight applications, size effects of foams have been studied intensively in literature, e. g. [3, 7, 12, 27, 28, 33]. In order to ensure the integrity of foam structures, thus models are required that are able to predict and simulate deformations and strength including size effects.

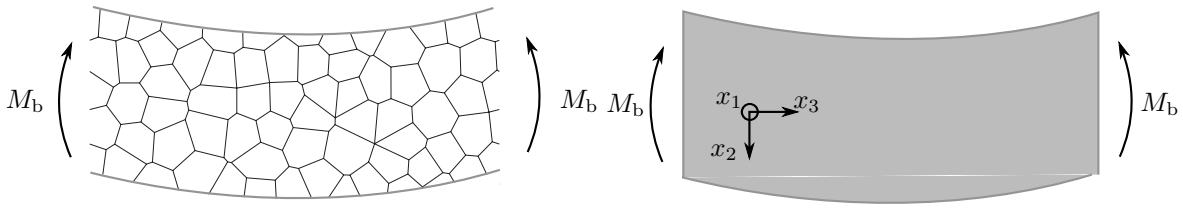

(a) Discrete microstructure (b) Homogenized micromorphic theory

Figure 1: Size-effects in bending

The microstructure of such foams can hardly be resolved discretely in computational simulations of whole components to account for size effects. Rather, extended continuum theories are desirable for this purpose containing the relevant microstructural length scale in the constitutive description, see Figure 1b.

Historically, the Cosserat continuum is the oldest theory meeting this requirement. In the Cosserat theory the rotations of a material point become independent macroscopic kinematic quantities giving rise to additional stress measures and balance equations. Later, Eringen and Suhubi [13] proposed the more general micromorphic continuum theory where the complete deformation tensor is a independent kinematic quantity called "microdeformation". In this context, Eringen entitled the contained special case of the Cosserat continuum as micropolar theory. Also other extended continuum theories are special cases of the micromorphic theory. For a classification of micromorphic theories, the reader is referred to Forest and Sievert [17]. However, the higher number of stress and strain quantities in extended continuum theories requires also an increasing number of constitutive laws and respective constitutive parameters. For instance, even for isotropic linear-elastic material, the number of constitutive parameters rises from two in classical theory to six in micropolar theory and even 18 in fully micromorphic theory. The experimental determination of such a large number of constitutive parameters for a particular material is of course very complex. Presumably due to the considerably lower number of parameters, first attempts to model size effects thus employed micropolar theory (e.g. [3, 14, 18, 27, 28, 33]).

Gauthier and Jahsman [18] pointed out the necessity to have analytical solutions for some micropolar boundary value problems in order to get an impression of the effects of the large number of constitutive parameters. Consequently, they provided solutions for torsion and bending which exhibit a size-effect. Based on this finding, Gauthier and Jahsman recommended to perform corresponding bending and torsion experiments with specimens of different cross section dimensions to identify the constitutive parameters. Subsequently, further analytical solutions for some bending and torsion problems of micropolar continua were derived [14, 22, 30, 31, 32]. However, Lakes [28] pointed out that micropolar theories are insufficient to describe some of the size effects which are observed with real foams like the dispersion of longitudinal waves and the particular size effect in bending. For this reason, Lakes [28] proposed to employ a fully micromorphic theory to capture all observed size effects. The problem is that even for linear-elastic isotropic material the number of material parameters to be determined rises to 18 compared to 6 for micropolar material.

Alternatively, the microdilatational continuum[1] is a theory were the volumetric strain becomes an additional macroscopic field quantity. This theory predicts size effects in bending as well as dispersion of longitudinal waves but neither the experimentally observed size effects under torsion nor dispersion of transversal waves [8, 10]. The microstretch continuum combines the micropolar and microdilatational approaches. It should thus be able to predict the observed size effects under bending and torsion as well as dispersion of longitudinal and transversal waves. Analytical solutions for bending and torsion of microstretch continua are available [9, 21]. However, to the author's knowledge no attempts have

[1] In the original literature, this approach is entitled "theory of porous elastic materials". This terminology is omitted here since all theories discussed here can be applied to porous elastic materials.

been made yet to identify the eight constitutive parameters for isotropic linear-elastic material from experiments.

The problems in identifying the huge number of constitutive parameters of extended continuum theories led to numerous activities to gain the parameters from homogenisation procedures. First studies focussed on micropolar continua [1, 4, 6, 11, 16, 29] or constrained micromorphic theories [2, 4, 5, 26, 35]. Fully micromorphic homogenisation schemes were applied to heterogeneous [15, 23] and foam-like elastic materials [20, 23, 24, 25]. In [15, 23, 24, 25] numerical methods were employed for the homogenisation, whereas a closed form solution was presented in [20]. Remarkably, although not excluded a priori, in the latter study the micropolar terms drop out leading to a microstrain continuum. The elastic microstrain model in [20] contains two parameters in addition to the classical ones: the porosity and the mean distance of pores, both having an intuitive physical meaning. In general, a microstrain continuum is assumed to be able to predict size effects under bending and torsion as well as dispersion of longitudinal and transversal waves. However, corresponding solutions of macroscopic boundary value problems for microstrain continua are not available yet to the author's knowledge. Thus, the aim of the present study is to derive analytical solutions for bending and torsion of the microstrain model for porous media. A comparison with corresponding experimental data from literature aims at rendering the predictive capabilities and limitations of the microstrain model.

2 Microstrain Model for Porous Media

Before coming to the solutions for bending and torsion, the micromorphic theory and the constitutive description for porous media shall be briefly reviewed. For details we refer to [17, 19, 20]. Regarding notation, scalars, vectors, second to forth order tensors are denoted by a, $\underline{\mathbf{b}}$, $\underset{\sim}{\mathbf{c}}$, $\underset{\approx}{\mathbf{d}}$ and $\underset{\approx}{\underset{\sim}{\mathbf{d}}}$, respectively. Single, double and triple contractions are indicated by $\cdot$, : and $\vdots$, respectively. They are computed from left to right, i.e. $\underset{\approx}{\underset{\sim}{\mathbf{d}}}\vdots\underset{\approx}{\underset{\sim}{\mathbf{e}}} = d_{ijk}e_{ijk}$ using the summation convention with d_{ijk} referring to the coordinates of tensor $\underset{\approx}{\underset{\sim}{\mathbf{d}}}$ in a Cartesian frame. The symbol $\otimes$ for the dyadic product is inserted only where confusions may arise, otherwise it is omitted. Furthermore, $\underline{\nabla}$ denotes the Nabla operator.

2.1 Kinematics

In micromorphic media, the microdeformation tensor $\underset{\sim}{\chi}$ becomes a primary kinematic quantity in addition to the displacement vector $\underline{\mathbf{U}}$. Within a small displacement framework, deformation measures are the usual macroscopic strain

$$\underset{\sim}{\varepsilon} = \frac{1}{2}(\underline{\nabla}\underline{\mathbf{U}} + \underline{\mathbf{U}} \otimes \underline{\nabla}), \tag{1}$$

the deformation difference

$$\underset{\sim}{\mathbf{e}} = \underset{\sim}{\mathbf{F}} - \underset{\sim}{\chi} \tag{2}$$

between macroscopic deformation gradient $\underset{\sim}{\mathbf{F}} = \underset{\sim}{\mathbf{I}} + \underline{\nabla}\underline{\mathbf{U}}$ and microdeformation $\underset{\sim}{\chi}$ as well as the microdeformation gradient

$$\underset{\approx}{\underset{\sim}{\mathbf{K}}} = \underset{\sim}{\chi} \otimes \underline{\nabla}. \tag{3}$$

2.2 Kinetics

The work-conjugate stresses to these deformation measures derive from a state potential $\Psi(\underset{\sim}{\varepsilon}, \underset{\sim}{\mathbf{e}}, \underset{\approx}{\underset{\sim}{\mathbf{K}}})$:

$$\underset{\sim}{\sigma} = \frac{\partial \Psi}{\partial \underset{\sim}{\varepsilon}}, \qquad \underset{\sim}{\mathbf{s}} = \frac{\partial \Psi}{\partial \underset{\sim}{\mathbf{e}}}, \qquad \underset{\approx}{\underset{\sim}{\mathbf{M}}} = \frac{\partial \Psi}{\partial \underset{\approx}{\underset{\sim}{\mathbf{K}}}}. \tag{4}$$

In absence of inertia or volume forces, the balance equations read

$$\left(\underset{\sim}{\sigma} + \underset{\sim}{\mathrm{s}}\right) \cdot \underline{\nabla} = 0 \tag{5}$$

$$\underset{\sim}{\mathrm{s}} + \underline{\underline{\mathbf{M}}} \cdot \underline{\nabla} = 0\,, \tag{6}$$

see e. g. [17, 19].

2.3 Constitutive Law

The state potential was derived by homogenisation in [20] for a medium with pores of volume fraction f as

$$\Psi = \frac{1}{2}(1-f)\underset{\sim}{\varepsilon} : \underset{\approx}{\mathbf{S}}^{(\mathrm{m})} : \underset{\sim}{\varepsilon} + \frac{R^2}{2} F^{\underline{\underline{\mathbf{K}}}}(f) \left(\underline{\underline{\mathbf{K}}}^{\mathrm{T}} : \underset{\approx}{\mathbf{S}}^{(\mathrm{m})} : \underline{\underline{\mathbf{K}}}\right) : \underline{\mathbf{I}} + \frac{1}{2} F^{\underline{\underline{\mathbf{ee}}}}(f) \underset{\sim}{\mathbf{e}} : \underset{\approx}{\mathbf{S}}^{(\mathrm{m})} : \underset{\sim}{\mathbf{e}} + F^{\underline{\varepsilon}\underline{\mathbf{e}}}(f) \underset{\sim}{\varepsilon} : \underset{\approx}{\mathbf{S}}^{(\mathrm{m})} : \underset{\sim}{\mathbf{e}}\,. \tag{7}$$

Therein, R denotes the radius of the unit cell which has to be interpreted as mean half distance between neighboring pores. Furthermore, $\underset{\approx}{\mathbf{S}}^{(\mathrm{m})}$ is the classical stiffness tensor of the matrix material. The dimensionless coefficients $F^{\underline{\underline{\mathbf{ee}}}}$, $F^{\underline{\varepsilon}\underline{\mathbf{e}}}$ and $F^{\underline{\underline{\mathbf{K}}}}$ depend on the porosity f and read for spherical voids

$$\begin{aligned} F^{\underline{\underline{\mathbf{ee}}}}(f) &= \frac{7}{12}\left[4 - 21f + 42f^{5/3} - 25f^{7/3}\right] \\ F^{\underline{\varepsilon}\underline{\mathbf{e}}}(f) &= \frac{7}{2} f \left(1 - f^{2/3}\right) \\ F^{\underline{\underline{\mathbf{K}}}}(f) &= \frac{1}{5}\left(1 - f^{5/3}\right)\,. \end{aligned} \tag{8}$$

According to (4), the linear-elastic constitutive relations are thus obtained from (7) as

$$\underset{\sim}{\sigma} = (1-f)\underset{\approx}{\mathbf{S}}^{(\mathrm{m})} : \underset{\sim}{\varepsilon} + F^{\underline{\varepsilon}\underline{\mathbf{e}}}(f) \underset{\approx}{\mathbf{S}}^{(\mathrm{m})} : \underset{\sim}{\mathbf{e}} \tag{9}$$

$$\underset{\sim}{\mathrm{s}} = F^{\underline{\underline{\mathbf{ee}}}}(f) \underset{\approx}{\mathbf{S}}^{(\mathrm{m})} : \underset{\sim}{\mathbf{e}} + F^{\underline{\varepsilon}\underline{\mathbf{e}}}(f) \underset{\approx}{\mathbf{S}}^{(\mathrm{m})} : \underset{\sim}{\varepsilon} \tag{10}$$

$$\underline{\underline{\mathbf{M}}} = R^2 F^{\underline{\underline{\mathbf{K}}}}(f) \underset{\approx}{\mathbf{S}}^{(\mathrm{m})} : \underline{\underline{\mathbf{K}}} \tag{11}$$

Note that in (7), the strain measures $\underset{\sim}{\varepsilon}$, $\underset{\sim}{\mathbf{e}}$ and $\underline{\underline{\mathbf{K}}}$ are always contracted twice with the symmetric tensor $\underset{\approx}{\mathbf{S}}^{(\mathrm{m})}$. Consequently, the skew-symmetric micropolar terms do not contribute which is why the formulation corresponds to a microstrain continuum.

For a homogeneous deformation field the microdeformation gradient $\underline{\underline{\mathbf{K}}}$ and thus the higher-order stress $\underline{\underline{\mathbf{M}}}$ vanish. The corresponding higher-order balance equation (6) then reduces to $\underset{\sim}{\mathrm{s}} = 0$. According to the constitutive law (10), $\underset{\sim}{\mathrm{s}} = 0$ corresponds to $\underset{\sim}{\mathbf{e}} = -F^{\underline{\varepsilon}\underline{\mathbf{e}}}/F^{\underline{\underline{\mathbf{ee}}}}\underset{\sim}{\varepsilon}$. Inserting this relation into constitutive relation (9) results in

$$\underset{\sim}{\sigma} = \left[1 - f - (F^{\underline{\varepsilon}\underline{\mathbf{e}}})^2/F^{\underline{\underline{\mathbf{ee}}}}\right] \underset{\approx}{\mathbf{S}}^{(\mathrm{m})} : \underset{\sim}{\varepsilon} \tag{12}$$

Thus, if higher order terms are negligible, i.e. if the deformation fields do not change significantly over distances comparable to the intrinsic length R, Eq. (5) of the microstrain theory reduces to the classical equilibrium condition $\underset{\sim}{\sigma} \cdot \underline{\nabla} = 0$ together with constitutive law (12). Note that both in (9) and (10) and consequently also in (12) all components of the respective stiffness tensors are affected by the void volume fraction f only by prefactors. Thus, the theory predicts e. g. that stiffnesses with respect to dilatational and deviatoric deformations are influenced by f in the same way. This fact is attributed to the fact that the boundary-value problem on the micro-scale for obtaining (9)–(11) was solved in [20] only approximately by Ritz' method with a cubic polynomial as ansatz. The solution may be improved in principle if additional higher-order terms are included, though, making it even more challenging to find a closed-form solution. Anyway, the aim of the present study is to evaluate the effects of the non-classical terms in (9)–(11), i. e. of those associated with the additional deformation measures $\underset{\sim}{\mathbf{e}}$ and $\underline{\underline{\mathbf{K}}}$.

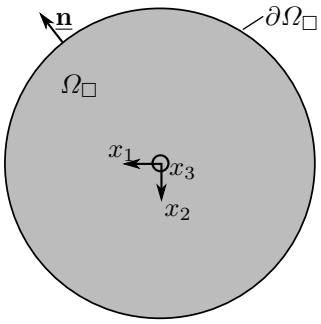

Figure 2: Cross section of beam

In the following, isotropic behavior of the matrix is assumed and thus the stiffness tensor $\overset{\approx}{\mathbf{S}}^{(\mathrm{m})}$ of the matrix material can be expressed in terms of both Lamé's constants $\mu^{(\mathrm{m})}$ and $\lambda^{(\mathrm{m})}$ as $\overset{\approx}{\mathbf{S}}^{(\mathrm{m})} = 2\mu^{(\mathrm{m})}\overset{\approx}{\mathbf{I}}^{\mathrm{s}} + \lambda^{(\mathrm{m})}\underset{\sim}{\underset{\sim}{\mathbf{II}}}$. According to (12), the macroscopic elastic constants of shear modulus and Young's modulus are thus obtained as $\mu = [1 - f - (F^{\varepsilon\underline{\mathbf{e}}})^2/F^{\underline{\mathbf{ee}}}]\mu^{(\mathrm{m})}$ and $E = [1 - f - (F^{\varepsilon\underline{\mathbf{e}}})^2/F^{\underline{\mathbf{ee}}}]E^{(\mathrm{m})}$ with $E^{(\mathrm{m})} = \mu^{(\mathrm{m})}(2\mu^{(\mathrm{m})} + 3\lambda^{(\mathrm{m})})/(\mu^{(\mathrm{m})} + \lambda^{(\mathrm{m})})$.

3 Bending

3.1 Arbitrary Cross Sections

We consider the pure bending of a beam with arbitrary cross section in the x_1-x_2-plane whose longitudinal axis coincides with the x_3-direction, see Figure 2. Preliminary studies of bending problems [18] for extended continuum theories have shown that the Euler-Bernoulli displacement field

$$\underline{\mathbf{U}} = w(x_3)\underline{\mathbf{b}}_2 + \alpha(x_3)x_2\underline{\mathbf{b}}_3 \text{ with } \alpha = -w' \tag{13}$$

remains valid. This is also the case for the present microstrain theory as will be shown in the following. In (13), $w(x_3)$ and $\alpha(x_3)$ denote deflection and rotation, respectively. Furthermore, $\underline{\mathbf{b}}_2$ and $\underline{\mathbf{b}}_3$ are Cartesian unit vectors and $(\circ)'$ refers to the derivative of a function with respect to its only scalar argument, i.e. here with respect to x_3. Inserting (13) into (1) yields the classical linear strain field

$$\underset{\sim}{\varepsilon} = \kappa x_2 \underline{\mathbf{b}}_3\underline{\mathbf{b}}_3 \text{ with } \kappa = \alpha' \,. \tag{14}$$

Due to the linearity of the problem, the microdeformation must be linearly related to the curvature κ. Furthermore, it is assumed to be directed also in x_3-x_3-direction. Thus, an ansatz

$$\underset{\sim}{\chi} = \underset{\sim}{\mathbf{I}} + \kappa g_{\mathrm{b}}(\underline{\mathbf{x}}_\square)\underline{\mathbf{b}}_3\underline{\mathbf{b}}_3 \tag{15}$$

is chosen with a function $g_{\mathrm{b}}(\underline{\mathbf{x}}_\square)$ depending only on the location $\underline{\mathbf{x}}_\square = x_1\underline{\mathbf{b}}_1 + x_2\underline{\mathbf{b}}_2$ in the cross section $\Omega_\square$. Inserting the strain and microdeformation from Eqs. (14) and (15) into constitutive laws (9) and (10) yields stresses

$$\underset{\sim}{\sigma} = E^{(\mathrm{m})}\kappa\left[(1 - f + F^{\varepsilon\underline{\mathbf{e}}}(f))\, x_2 - g_{\mathrm{b}}(\underline{\mathbf{x}}_\square)F^{\varepsilon\underline{\mathbf{e}}}(f)\right]\underline{\mathbf{b}}_3\underline{\mathbf{b}}_3 \tag{16}$$

$$\underset{\sim}{\mathbf{s}} = E^{(\mathrm{m})}\kappa\left[(F^{\underline{\mathbf{ee}}}(f) + F^{\varepsilon\underline{\mathbf{e}}}(f))\, x_2 - g_{\mathrm{b}}(\underline{\mathbf{x}}_\square)F^{\underline{\mathbf{ee}}}(f)\right]\underline{\mathbf{b}}_3\underline{\mathbf{b}}_3 \tag{17}$$

under the usual assumption for bending that Poisson's ratio and thus the second Lamé parameter $\lambda^{(\mathrm{m})}$ are zero. Equilibrium condition (5) thus reduces to the requirement that the curvature κ has to be constant. Under this condition, the microdeformation gradient is obtained from (15) as

$$\underset{\sim}{\underset{\sim}{\mathbf{K}}} = \underset{\sim}{\chi} \otimes \underline{\nabla} = \kappa\underline{\mathbf{b}}_3\underline{\mathbf{b}}_3\underline{\nabla}_\square g_{\mathrm{b}}(\underline{\mathbf{x}}_\square) \tag{18}$$

wherein the in-plane Nabla operator was defined as $\underline{\nabla}_\square g_\mathrm{b} = g_{\mathrm{b},x_1}\underline{\mathbf{b}}_1 + g_{\mathrm{b},x_2}\underline{\mathbf{b}}_2$. Subsequently, the higher order stress is calculated from (11) as

$$\underline{\underline{\underline{\mathbf{M}}}} = E^{(\mathrm{m})}\kappa R^2 F^{\underline{\underline{\mathbf{K}}}}(f)\underline{\mathbf{b}}_3\underline{\mathbf{b}}_3\underline{\nabla}_\square g_\mathrm{b}(\underline{\mathbf{x}}_\square)\,. \tag{19}$$

With difference stress $\underline{\underline{\mathbf{s}}}$ from (17), this result can be inserted into the higher order equilibrium condition (6) giving

$$E^{(\mathrm{m})}\kappa\left[R^2 F^{\underline{\underline{\mathbf{K}}}}\Delta_\square g_\mathrm{b} - F^{\underline{\underline{\mathbf{ee}}}} g_\mathrm{b} + \left(F^{\underline{\underline{\mathbf{ee}}}} + F^{\varepsilon\underline{\underline{\mathbf{e}}}}\right)x_2\right]\underline{\mathbf{b}}_3\underline{\mathbf{b}}_3 = 0\,. \tag{20}$$

Consequently, the term in square brackets with the in-plane Laplace operator $\Delta_\square g_\mathrm{b} = \underline{\nabla}_\square \cdot \underline{\nabla}_\square g_\mathrm{b}$ has to vanish. This expressions constitutes an inhomogeneous PDE of Helmholtz-type for the microbending function $g_\mathrm{b}(x_1, x_2)$ with the classical solution x_2 as right-hand side term. Corresponding boundary conditions $\underline{\nabla}_\square g_\mathrm{b} \cdot \underline{\mathbf{n}} = 0$ result from the requirement that higher order tractions $\underline{\underline{\underline{\mathbf{M}}}} \cdot \underline{\mathbf{n}} = 0$ vanish on the surface $\partial\Omega_\square$ employing expression (19) for $\underline{\underline{\underline{\mathbf{M}}}}$. It is convenient to split-up the solution into a particular integral and a normalized homogeneous solution

$$g_\mathrm{b}(x_1, x_2) = \frac{F^{\underline{\underline{\mathbf{ee}}}} + F^{\varepsilon\underline{\underline{\mathbf{e}}}}}{F^{\underline{\underline{\mathbf{ee}}}}}\left[x_2 - \hat{R}_\mathrm{b} g_{\mathrm{b,h}}\underbrace{\left(\underline{\mathbf{x}}_\square/\hat{R}_\mathrm{b}\right)}_{=:\bar{\underline{\mathbf{x}}}_\square}\right] \tag{21}$$

introducing the characteristic intrinsic length scale of bending

$$\hat{R}_\mathrm{b} = R\sqrt{\frac{F^{\underline{\underline{\mathbf{K}}}}(f)}{F^{\underline{\underline{\mathbf{ee}}}}(f)}}\,. \tag{22}$$

Inserting (21) into constitutive law (17), gives $\underline{\underline{\mathbf{s}}} = E^{(\mathrm{m})}\kappa\left(F^{\underline{\underline{\mathbf{ee}}}}(f) + F^{\varepsilon\underline{\underline{\mathbf{e}}}}(f)\right)\hat{R}_\mathrm{b} g_{\mathrm{b,h}}(\bar{\underline{\mathbf{x}}}_\square)\underline{\mathbf{b}}_3\underline{\mathbf{b}}_3$ demonstrating that the function $g_{\mathrm{b,h}}(\bar{\underline{\mathbf{x}}}_\square)$ is directly related to the difference stress $\underline{\underline{\mathbf{s}}}$. Finally, the boundary value problem for $g_{\mathrm{b,h}}(\bar{\underline{\mathbf{x}}}_\square)$ results from (20) and (21):

$$\bar{\Delta}_\square g_{\mathrm{b,h}} - g_{\mathrm{b,h}} = 0 \text{ in } \bar{\Omega}_\square \tag{23}$$

$$\bar{\underline{\nabla}}_\square g_{\mathrm{b,h}} \cdot \underline{\mathbf{n}} = \underline{\mathbf{b}}_2 \cdot \underline{\mathbf{n}} \text{ on } \partial\bar{\Omega}_\square\,. \tag{24}$$

Having solved this problem, the bending moment can be computed from the tractions normal to the cross section as

$$\begin{aligned} M_\mathrm{b} &= \int_{\Omega_\square} x_2\left(\underline{\underline{\sigma}} + \underline{\underline{\mathbf{s}}}\right) : \underline{\mathbf{b}}_3\underline{\mathbf{b}}_3\,\mathrm{d}A \\ &= \underbrace{E^{(\mathrm{m})}\left(1 - f - \frac{\left(F^{\varepsilon\underline{\underline{\mathbf{e}}}}\right)^2}{F^{\underline{\underline{\mathbf{ee}}}}}\right)}_{=E}\kappa\left[\underbrace{\int_{\Omega_\square} x_2^2\,\mathrm{d}A}_{=I_\mathrm{b}} + \hat{R}_\mathrm{b}^4\frac{\left(F^{\underline{\underline{\mathbf{ee}}}} + F^{\varepsilon\underline{\underline{\mathbf{e}}}}\right)^2}{(1-f)\,F^{\underline{\underline{\mathbf{ee}}}} - \left(F^{\varepsilon\underline{\underline{\mathbf{e}}}}\right)^2}\int_{\Omega_\square}\bar{x}_2 g_{\mathrm{b,h}}(\bar{\underline{\mathbf{x}}}_\square)\,\mathrm{d}\bar{A}\right]\,. \end{aligned} \tag{25}$$

A comparison with (12) shows, that the prefactor of the bracket corresponds to the macroscopic Young's modulus E. Besides the area moment of inertia I_b, the square bracket in (25) contains additional microstrain contributions. However, these additional contributions vanish for $\hat{R}_\mathrm{b} = 0$ thus recovering the classical solution in this limit case.

With the split-up (21), the normal stresses in the ligament from (16) can be also rewritten as

$$\underline{\underline{\sigma}} = E\kappa\left[x_2 + \hat{R}_\mathrm{b}\frac{F^{\varepsilon\underline{\underline{\mathbf{e}}}}\left(F^{\underline{\underline{\mathbf{ee}}}} + F^{\varepsilon\underline{\underline{\mathbf{e}}}}\right)}{(1-f)F^{\underline{\underline{\mathbf{ee}}}} - (F^{\varepsilon\underline{\underline{\mathbf{e}}}})^2} g_{\mathrm{b,h}}(\bar{\underline{\mathbf{x}}}_\square)\right]\underline{\mathbf{b}}_3\underline{\mathbf{b}}_3\,. \tag{26}$$

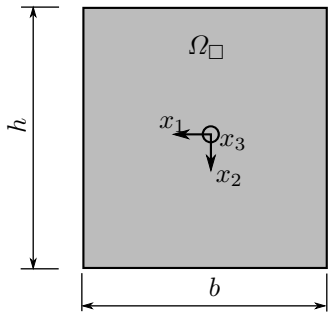

Figure 3: Rectangular cross section

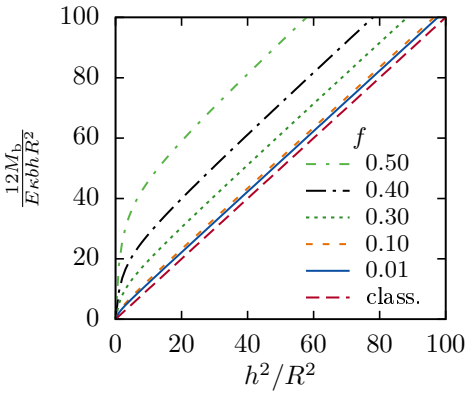

Figure 4: Normalized bending stiffness for rectangular cross section

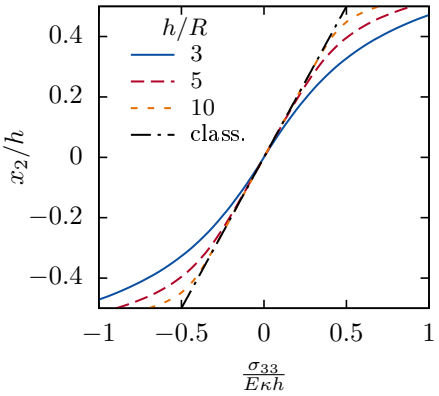

Figure 5: Distribution of bending stress over a rectangular cross section for $f = 0.4$

3.2 Rectangular Cross Section

For a beam with rectangular cross section as sketched in Figure 3, the area moment of inertia amounts to $I_\mathrm{b} = \frac{bh^3}{12}$. The ansatz $g_\mathrm{b,h} = g_\mathrm{b,h}(x_2/\hat{R}_\mathrm{b})$ for the homogeneous part of the bending function reduces PDE (23) to an ODE

$$g''_\mathrm{b,h} - g_\mathrm{b,h} = 0\,. \tag{27}$$

With the ansatz, boundary condition (24) is fulfilled identically at the left and right surfaces $x_1 = \pm b/2$. At the top and bottom surfaces, the boundary condition becomes $g'_\mathrm{b,h}(\pm h/(2\hat{R}_\mathrm{b})) = 1$ resulting in a solution $g_\mathrm{b,h} = \sinh(x_2/\hat{R}_\mathrm{b})/\cosh(h/(2\hat{R}_\mathrm{b}))$. Inserting it into (25) yields

$$M_\mathrm{b} = \kappa E \frac{bh}{12}\left[h^2 + 12\frac{\left(F^{\underline{\underline{\mathbf{ee}}}} + F^{\underline{\underline{\varepsilon}}\mathbf{e}}\right)^2}{(1-f)\,F^{\underline{\underline{\mathbf{ee}}}} - \left(F^{\underline{\underline{\varepsilon}}\mathbf{e}}\right)^2}\hat{R}_\mathrm{b}^2\left(1 - \frac{2\hat{R}_\mathrm{b}}{h}\tanh\frac{h}{2\hat{R}_\mathrm{b}}\right)\right]. \tag{28}$$

Via the coefficients $F^{\underline{\underline{\mathbf{ee}}}}$ and $F^{\underline{\underline{\varepsilon}}\mathbf{e}}$ and the definition of $\hat{R}_\mathrm{b}$ in (22), the predicted size effect thus depends on the porosity f. This size effect can be illustrated by plotting the bending stiffness M_b/κ in a normalized way versus h^2 as proposed by Gauthier and Jahsman [18]. Such a plot is provided in Figure 4 for different values of f in such a normalization that the classical solution corresponds to a line through the origin with unity slope. The plot shows that the predicted size effect depends strongly on the porosity f. For $f \gtrsim 0.3$, it is distinct even for heights h considerably larger than the half void distance R whereas it vanishes almost for small f.

The bending stresses according to (26) are plotted in Figure 5 for some parameter sets. It indicates that in the center, the stresses follow the classical solution whereas a deviating boundary layer is formed

at the top and bottom surfaces. The deviations from the classical solution become the stronger, the smaller the height h is compared to the material length R.

3.3 Circular Cross Section

For a circular cross section of radius a as shown in Figure 2 it is advantageous to switch to a polar coordinate system. In general, the solution of the in-plane problem (23)–(24) can be expanded as Fourier series in terms of the polar angle φ. However, the only non-homogeneous term stems from boundary condition (24) which reads $\bar{\nabla}_{\square} g_{\mathrm{b,h}} \cdot \underline{\mathbf{n}} = \underline{\mathbf{b}}_2 \cdot \underline{\mathbf{n}} = \sin\varphi$ at the surface $r = a$. Thus, it is sufficient to consider the terms with $\sin\varphi$. Consequently, we chose

$$g_{\mathrm{b,h}}(\bar{\underline{\mathbf{x}}}_{\square}) = g_{\mathrm{r}}(\bar{r}) \sin\varphi \tag{29}$$

leaving open only the dependency on the normalized radial coordinate $\bar{r} = r/\hat{R}_{\mathrm{b}}$. Having transformed the Laplace operator in (23) to polar coordinates, we thus obtain

$$\frac{\sin\varphi}{\bar{r}^2}\left[\bar{r}^2 g_{\mathrm{r}}'' + \bar{r} g_{\mathrm{r}}' - \left(1+\bar{r}^2\right) g_{\mathrm{r}}\right] = 0\,. \tag{30}$$

The bracketed term has to vanish leading to a solution $g_{\mathrm{r}} = c_1 I_1(\bar{r}) + c_2 K_1(\bar{r})$ in terms of modified Bessel functions of first order. The modified function of second kind $K_1(\bar{r})$ is unbounded at $\bar{r} = 0$ requiring $c_2 = 0$. Constant c_1 is determined from boundary condition (24) corresponding to $g_{\mathrm{r}}'\left(\frac{a}{\hat{R}_{\mathrm{b}}}\right) = 1$. Thus, the homogeneous bending function for a circular cross section is

$$g_{\mathrm{b,h}}(\bar{\underline{\mathbf{x}}}_{\square}) = \sin\varphi \frac{2 I_1(\bar{r})}{I_0\left(\frac{a}{\hat{R}_{\mathrm{b}}}\right) + I_2\left(\frac{a}{\hat{R}_{\mathrm{b}}}\right)}\,. \tag{31}$$

With $I_{\mathrm{b}} = \frac{\pi}{4} a^4$, the bending moment amounts to

$$M_{\mathrm{b}} = \kappa E \frac{\pi a^2}{4}\left[a^2 + 8 \frac{\left(F^{\underset{\sim}{\mathbf{ee}}} + F^{\underset{\sim}{\varepsilon}\mathbf{e}}\right)^2}{(1-f)\, F^{\underset{\sim}{\mathbf{ee}}} - \left(F^{\underset{\sim}{\varepsilon}\mathbf{e}}\right)^2} \hat{R}_{\mathrm{b}}^2 \frac{I_2\left(\frac{a}{\hat{R}_{\mathrm{b}}}\right)}{I_0\left(\frac{a}{\hat{R}_{\mathrm{b}}}\right) + I_2\left(\frac{a}{\hat{R}_{\mathrm{b}}}\right)}\right]\,. \tag{32}$$

A plot of (32) looks similar to the results for a rectangular cross section in Figure 4 and is thus omitted here. Instead, the predicted increase of bending stiffness for circular and square (i.e. rectangular with $b = h$) cross sections are compared in Figure 6 by plotting the stiffness, normalized by the prediction EI_{b} of classical theory, versus the cross sectional area A. The figure shows, that the predicted size effects are almost identical for both shapes. Only minor differences are observed for increased porosities $f \gtrsim 0.30$.

4 Torsion

According to Saint Venant's classical theory, torsion of prismatic rods of arbitrary cross section will result in warping. Even in classical theory, this requires the solution of a Poisson problem for determining the stress potential or a warping function. For this reason we consider only non-warping circular cross sections under torsion. In section 3.1 it was shown for bending, that the displacement field of the classical theory remains valid also for the microstrain continuum. That is why we adopt the classical Navier solution $\underline{\mathbf{U}} = r\alpha(x_3)\underline{\mathbf{b}}_{\varphi}$ yielding strains according to (1) of

$$\underset{\sim}{\varepsilon} = \frac{1}{2} r\vartheta\left(\underline{\mathbf{b}}_3\underline{\mathbf{b}}_{\varphi} + \underline{\mathbf{b}}_3\underline{\mathbf{b}}_{\varphi}\right) \tag{33}$$

with the twist $\vartheta = \alpha'$. Due to the linearity and axisymmetry of the problem, an ansatz

$$\underset{\sim}{\chi} = \underset{\sim}{\mathbf{I}} + \frac{1}{2}\vartheta g_{\mathrm{t}}(r)\left(\underline{\mathbf{b}}_3\underline{\mathbf{b}}_{\varphi} + \underline{\mathbf{b}}_3\underline{\mathbf{b}}_{\varphi}\right) \tag{34}$$

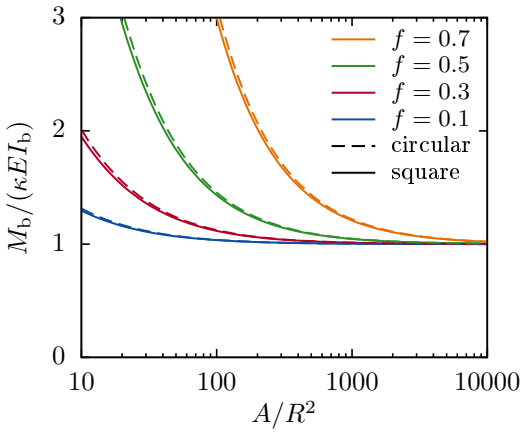

Figure 6: Relative bending stiffness of circular and square cross sections in dependence of cross sectional area A and porosity f

is chosen for the microdeformation with a function $g_\mathrm{t}(r)$ to be determined. Correspondingly, stresses

$$\underset{\sim}{\varrho} = \mu^{(\mathrm{m})}\vartheta\left[r\left(1-f+F^{\underset{\sim}{\varepsilon}\mathbf{e}}(f)\right) - g_\mathrm{t}(r)F^{\underset{\sim}{\varepsilon}\mathbf{e}}(f)\right]\left(\underline{\mathbf{b}}_3\underline{\mathbf{b}}_\varphi + \underline{\mathbf{b}}_3\underline{\mathbf{b}}_\varphi\right) \tag{35}$$

$$\underset{\sim}{\mathbf{s}} = \mu^{(\mathrm{m})}\vartheta\left[r\left(F^{\underset{\sim}{\mathbf{e}}\underset{\sim}{\mathbf{e}}}(f)+F^{\underset{\sim}{\varepsilon}\mathbf{e}}(f)\right) - g_\mathrm{t}(r)F^{\underset{\sim}{\mathbf{e}}\underset{\sim}{\mathbf{e}}}(f)\right]\left(\underline{\mathbf{b}}_3\underline{\mathbf{b}}_\varphi + \underline{\mathbf{b}}_3\underline{\mathbf{b}}_\varphi\right) \tag{36}$$

are obtained from constitutive laws (9) and (10). Inserting $\underset{\sim}{\varrho}$ and $\underset{\sim}{\mathbf{s}}$ into equilibrium condition (5) leads to the condition that the twist ϑ must be constant. In this case, a higher order stress of

$$\underset{\approx}{\mathbf{M}} = \mu^{(\mathrm{m})}\vartheta R^2 F^{\underline{\underline{\mathbf{K}}}}(f)\left[g_\mathrm{t}'(r)\left(\underline{\mathbf{b}}_3\underline{\mathbf{b}}_\varphi + \underline{\mathbf{b}}_\varphi\underline{\mathbf{b}}_3\right)\underline{\mathbf{b}}_r - \frac{g_\mathrm{t}(r)}{r}\left(\underline{\mathbf{b}}_3\underline{\mathbf{b}}_r + \underline{\mathbf{b}}_r\underline{\mathbf{b}}_3\right)\underline{\mathbf{b}}_\varphi\right] \tag{37}$$

is obtained from (11). The higher order equilibrium condition (6) thus reads

$$0 = \mu^{(\mathrm{m})}\vartheta\left\{R^2 F^{\underline{\underline{\mathbf{K}}}}\left[g_\mathrm{t}''(r) + \frac{g_\mathrm{t}'(r)}{r} - \frac{g_\mathrm{t}(r)}{r^2}\right] - F^{\underset{\approx}{\mathbf{e}}\underset{\sim}{\mathbf{e}}}g_\mathrm{t}(r) + \left(F^{\underset{\approx}{\mathbf{e}}\underset{\sim}{\mathbf{e}}} + F^{\underset{\sim}{\varepsilon}\mathbf{e}}\right)r\right\}\left(\underline{\mathbf{b}}_3\underline{\mathbf{b}}_\varphi + \underline{\mathbf{b}}_3\underline{\mathbf{b}}_\varphi\right) \tag{38}$$

with the consequence that the expression in curly brackets has to vanish. Similar to (21), it is useful to split up the torsion function in a particular integral and a normalized homogeneous solution:

$$g_\mathrm{t}(r) = \frac{F^{\underset{\approx}{\mathbf{e}}\underset{\sim}{\mathbf{e}}} + F^{\underset{\sim}{\varepsilon}\mathbf{e}}}{F^{\underset{\approx}{\mathbf{e}}\underset{\sim}{\mathbf{e}}}}\left[r - \hat{R}_\mathrm{b} g_{\mathrm{t,h}}\left(\frac{r}{\hat{R}_\mathrm{b}}\right)\right] \tag{39}$$

This yields the same modified Bessel ODE (30) as for bending of a circular cross section. Furthermore, the requirement for the higher order tractions to vanish at the surface $\underset{\approx}{\mathbf{M}}(r=a)\cdot\underset{\sim}{\mathbf{e}}_r = \underset{\sim}{\mathbf{0}}$ yields the same boundary condition $g_{\mathrm{t,h}}'\left(a/\hat{R}_\mathrm{b}\right) = 1$ as for bending. Consequently, the normalized solution

$$g_{\mathrm{t,h}}(\bar{r}) = \frac{2I_1\left(\frac{r}{\hat{R}_\mathrm{b}}\right)}{I_0\left(\frac{a}{\hat{R}_\mathrm{b}}\right) + I_2\left(\frac{a}{\hat{R}_\mathrm{b}}\right)}$$

is also the same as for bending. Reinserting this solution into stresses (35)–(36) allows to compute the torsion moment $M_\mathrm{t} = \int\limits_{\Omega_\square}\left(\underset{\sim}{\varrho} + \underset{\sim}{\mathbf{s}}\right)r : \underline{\mathbf{b}}_3\underline{\mathbf{b}}_\varphi\,\mathrm{d}A$

$$M_\mathrm{t} = \vartheta\mu\frac{\pi a^2}{2}\left[a^2 + 8\frac{\left(F^{\underset{\approx}{\mathbf{e}}\underset{\sim}{\mathbf{e}}} + F^{\underset{\sim}{\varepsilon}\mathbf{e}}\right)^2}{(1-f)F^{\underset{\approx}{\mathbf{e}}\underset{\sim}{\mathbf{e}}} - \left(F^{\underset{\sim}{\varepsilon}\underset{\sim}{\mathbf{e}}}\right)^2}\hat{R}_\mathrm{b}^2\frac{I_2\left(\frac{a}{\hat{R}_\mathrm{b}}\right)}{I_0\left(\frac{a}{\hat{R}_\mathrm{b}}\right) + I_2\left(\frac{a}{\hat{R}_\mathrm{b}}\right)}\right]. \tag{40}$$

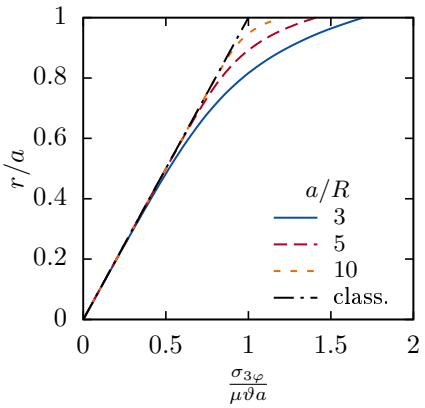

Figure 7: Distribution of shear stress in a cylinder under torsion for $f = 0.4$

As might be anticipated from the equivalence of the normalized solutions, the bracketed term in (40), which describes the size effect relative to the classical theory, is the same as for bending in (32). Remarkably, even the relevant internal length $\hat{R}_\mathrm{b}$ coincide for torsion and bending of cylinders. The distribution of the stresses

$$\underset{\sim}{\sigma} = \mu\vartheta \left[r + \hat{R}_\mathrm{b} \frac{F^{\varepsilon\mathbf{e}} \left(F^{\mathbf{ee}}_{\sim\sim} + F^{\varepsilon\mathbf{e}} \right)}{(1-f)\, F^{\mathbf{ee}}_{\sim\sim} - \left(F^{\varepsilon\mathbf{e}} \right)^2} \frac{2 I_1\left(\frac{r}{\hat{R}_\mathrm{b}}\right)}{I_0\left(\frac{a}{\hat{R}_\mathrm{b}}\right) + I_2\left(\frac{a}{\hat{R}_\mathrm{b}}\right)} \right] \left(\underline{\mathbf{b}}_3 \underline{\mathbf{b}}_\varphi + \underline{\mathbf{b}}_3 \underline{\mathbf{b}}_\varphi \right) \tag{41}$$

is plotted over radius r in Figure 7 exhibiting a similar picture as the normal stresses under bending of a beam with rectangular cross section in Figure 5.

5 Comparison with Experimental Results for Closed-Cell Foams

It shall be recalled at this point that the microstrain theory of elasticity, which is considered in the present paper, was derived from a homogenisation procedure. Thus, as constitutive parameters it requires only the porosity f and the intrinsic length R as half mean distance of pores in addition to the classical constants of elasticity E and μ. All these parameters have a clear physical meaning and can thus be measured directly. Vice versa this means that if these parameters were measured for a particular material, the theory *predicts* size effects under bending and torsion. In this section it is to be evaluated whether these predictions are qualitatively and quantitatively realistic.

For this purpose, the extensive experimental studies on size effects for elastic bending and torsion of closed-cell polymeric foam Rohacell WF300 by Anderson and Lakes [3] are considered. From the published mass density of the foam, the porosity can be estimated as $f = 0.62$. Furthermore, in [3] a cell size of 0.65 mm is given for this material. Although no exact definition of the "cell size" is provided, the half mean distance between pores should be $R \approx$ cell size$/2 \approx 0.3$ mm. Lacking the elastic properties $\mu^{(\mathrm{m})}$ and $\lambda^{(\mathrm{m})}$ of the matrix material, the effective macroscopic values of Young's modulus $E = 650$ MPa and shear modulus $\mu = 295$ MPa are employed directly as average of the values published in [3].

The predictions of the microstrain theory with the derived analytical solutions from (28) for bending of a square cross section $b = h$ are compared to corresponding experimental stiffness data for different cross section dimensions h. Figure 8 shows that the predictions correspond qualitatively and quantitatively to the measurements. Since the value $R = 0.3$ mm is an estimate only, graphs for $R = 0.2$ mm and $R = 0.4$ mm are plotted as well for comparison.

With the same foam material, Anderson and Lakes [3] performed also bending and torsion experiments with cylinders. The results in sections 3.3 and 4 showed that the present theory predicts an identical relative size effect in this case. A correspondingly normalized plot in Figure 9 confirms that this is indeed observed in experiments. However, the best fit of the theory with experiments would be obtained for the circular cross section for $R \approx 0.2$ mm compared to $R \approx 0.3$ mm for rectangular cross sections.

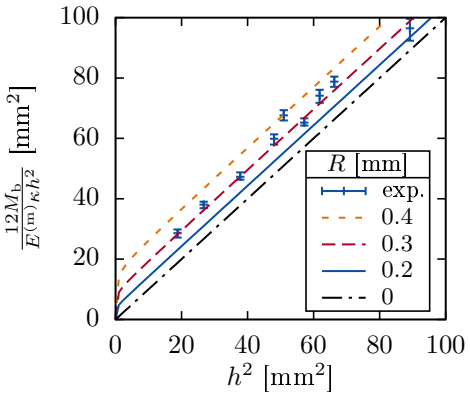

Figure 8: Comparison of bending stiffness for square cross section to experimental data from [3]

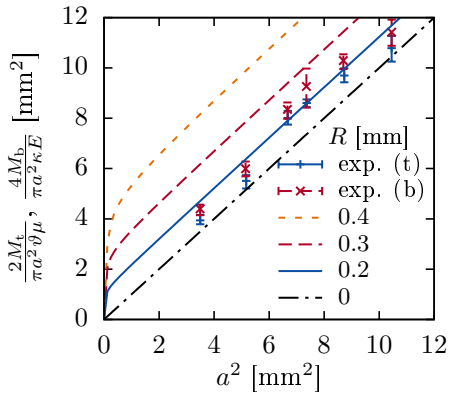

Figure 9: Comparison of bending (b) and torsion (t) stiffnesses for circular cross sections to experimental data from [3]

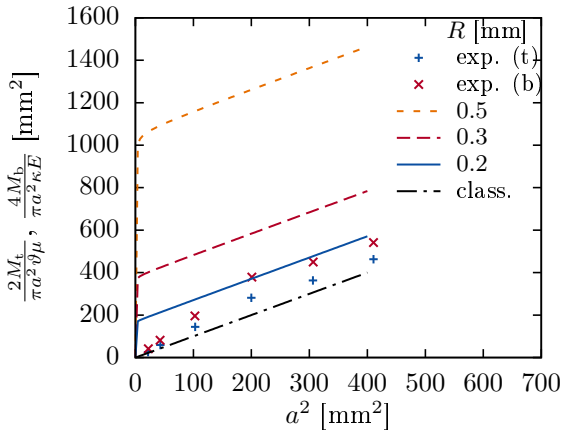

Figure 10: Comparison of bending (b) and torsion (t) stiffnesses of cylinders to experimental data of high-porosity polysterene foam from [28]

Lakes [28] performed also similar investigations on the size effect on a closed-cell polysterene foam. For this material, the cell size is given with approximately 1 mm which would correspond to $R \approx 0.5\,\mathrm{mm}$. From the published mass density, a porosity of $f \approx 0.96$ is expected. A normalized plot of bending and torsion stiffnesses measured for this material with cylinders of different diameter is provided in Figure 10. In contrast to the Rohacell foam in Figure 9, the normalized data for bending and torsion in Figure 10 deviate considerably, an effect which is in contradiction with the derived solutions. Furthermore, the present theory overestimates the size effect considerably for the polysterene foam with such a large porosity (compare also the horizontal shift of the initiation of the size effect in Figure 6 with increasing f).

It was reported already in [20], that the theory overestimated the size effect for shearing of thin layers for high porosities. In open-cell foams, a non-stress carrying layer may be formed by struts ending at the surface which is why reduced are even inverse size effects can be observed with such materials [34]. Possibly, similar effects are relevant for closed-cell foams with large porosities. Furthermore, it has to be recalled that the constitutive relation of the employed microstrain theory was derived [20] in only by an approximate procedure. Thus, the present microstrain theory seems to be adequate for elastic size effects of closed-cell foams with moderate porosities $f \lesssim 0.7$.

6 Summary and Conclusions

In the present study, the analytical solutions for pure bending and (warping-free) torsion are derived for an elastic microstrain continuum whose constitutive laws for porous media were derived by a homogenisation procedure in a previous study [20]. For the bending case, the problem reduces to a plane Helmholtz problem in the cross section, whose solutions for rectangular and circular cross sections are provided. For torsion, the solution is presented for circular cross sections. All solutions exhibit a term in addition to the classical solution that contains the intrinsic length scale of the material. For the constitutive parameters gained by homogenisation, the intrinsic length scales are the same for torsion and bending. However, this intrinsic length depends strongly on the porosity. The presence of an intrinsic length scale in the solutions for bending and torsion reflects a size effect which is well-known from experiments with foam structures. A comparison with corresponding data from literature reveals that the predictions of the microstrain theory match qualitatively and quantitatively to experimental findings for a closed-cell polymeric foam with a porosity of about 60%. The derived closed-form solution for the relative increase of bending stiffness for rectangular cross sections can also be adopted to the bending of plates of foam material, a topic that is relevant if a foam material is used as core in sandwich constructions. However, the magnitude of the observed size effect for a polysterene foam with a porosity of 95% is considerably overestimated by the theory. This discrepancy for high porosities may stem from the fact that in the homogenisation procedure the boundary value problem on the microscale was solved only approximately. Furthermore, the treatment of the pore in the relation between microscale displacements and macroscopic higher-order kinematic quantities in the homogenisation might require further research. Anyway, the present microstrain theory allows reasonable predictions of the size effect of closed-cell foams for moderate porosities $f \lesssim 0.7$.

References

[1] D. Addessi, E. Sacco, and A. Paolone. "Cosserat model for periodic masonry deduced by nonlinear homogenization". In: *Eur. J. Mech. A-Solid.* 29.4 (2010), pp. 724–737.

[2] G. Adomeit. "Determination of Elastic Constants of a Structured Material". In: *Mechanics of Generalized Continua.* Ed. by E. Kröner. Berlin/Heidelberg: Springer-Verlag, 1968, pp. 80–82.

[3] W. B. Anderson and R. S. Lakes. "Size effects due to Cosserat elasticity and surface damage in closed-cell polymethacrylimide foam". In: *J. Mater. Sci.* 29.24 (1994), pp. 6413–6419.

[4] D. Bigoni and W. J. Drugan. "Analytical Derivation of Cosserat Moduli via Homogenization of Heterogeneous Elastic Materials". In: *J. Appl. Mech.* 74.4 (2006), pp. 741–753.

[5] F. Bouyge, I. Jasiuk, and M. Ostoja-Starzewski. "A micromechanically based couple-stress model of an elastic two-phase composite". In: *Int. J. Solids. Struct.* 38.10–13 (Mar. 2001), pp. 1721–1735.

[6] D. Branke et al. "Obtaining Cosserat material parameters by homogenization of a Cauchy continuum". In: *Proc. Appl. Math. Mech.* 9.1 (2009), pp. 425–426.

[7] C. Chen and N. A. Fleck. "Size effects in the constrained deformation of metallic foams". In: *J. Mech. Phys. Solids.* 50.5 (2002), pp. 955–977.

[8] S. C. Cowin and J. W. Nunziato. "Linear elastic materials with voids". In: *J. Elasticity.* 13.2 (1983), pp. 125–147.

[9] S. De Cicco and L. Nappa. "Torsion and flexure of microstretch elastic circular cylinders". In: *Int. J. Eng. Sci.* 35.6 (1997), pp. 573–583.

[10] F. Dell'Isola and R. C. Batra. "Saint-Venant's Problem for Porous Linear Elastic Materials". In: *J. Elasticity.* 47.1 (1997), pp. 73–81.

[11] S. Diebels and H. Steeb. "Stress and couple stress in foams". In: *Comp. Mater. Sci.* 28.3-4 (2003), pp. 714–722.

[12] T. Dillard, S. Forest, and P. Ienny. "Micromorphic continuum modelling of the deformation and fracture behaviour of nickel foams". In: *Eur. J. Mech. A-Solid.* 25.3 (2006), pp. 526–549.

[13] A. C. Eringen and E. S. Suhubi. "Nonlinear theory of simple micro-elastic solids–I". In: *Int. J. Eng. Sci.* 2.2 (1964), pp. 189–203.

[14] N. Fleck et al. "Strain gradient plasticity: Theory and experiment". In: *Acta. Metall. Mater.* 42.2 (1994), pp. 475–487.

[15] S. Forest and D. K. Trinh. "Generalized continua and non-homogeneous boundary conditions in homogenisation methods". In: *Z. Angew. Math. Mech.* 91.2 (2011), pp. 90–109.

[16] S. Forest and K. Sab. "Cosserat overall modeling of heterogeneous materials". In: *Mech. Res. Commun.* 25.4 (1998), pp. 449–454.

[17] S. Forest and R. Sievert. "Nonlinear microstrain theories". In: *Int. J. Solids. Struct.* 43.24 (2006), pp. 7224–7245.

[18] R. D. Gauthier and W. E. Jahsman. "A Quest for Micropolar Elastic Constants". In: *J. Appl. Mech.* 42.2 (1975), pp. 369–374.

[19] P. Germain. "The method of virtual power in continuum mechanics. Part 2: Microstructure". In: *Siam. J. Appl. Math.* 25.3 (1973), pp. 556–575.

[20] G. Hütter, U. Mühlich, and M. Kuna. "Micromorphic homogenization of a porous medium: elastic behavior and quasi-brittle damage". In: *Continuum. Mech. Therm.* 27 (2015), pp. 1059–1072.

[21] D. Ieşan and L. Nappa. "Saint-Venant's problem for microstretch elastic solids". In: *Int. J. Eng. Sci.* 32.2 (1994), pp. 229–236.

[22] D. Ieşan. "Torsion of micropolar elastic beams". In: *Int. J. Eng. Sci.* 9.11 (1971), pp. 1047–1060.

[23] R. Jänicke and H. Steeb. "Minimal loading conditions for higher order numerical homogenisation schemes". In: *Arch. Appl. Mech.* 82.8 (2012), pp. 1075–1088.

[24] R. Jänicke et al. "Micromorphic two-scale modelling of periodic grid structures". In: *Int. J. Multiscale Com.* 11.2 (2013), pp. 161–176.

[25] R. Jänicke et al. "Two-scale modelling of micromorphic continua". In: *Continuum. Mech. Therm.* 21.4 (2009), pp. 297–315.

[26] V. Kouznetsova, M. G. D. Geers, and W. A. M. Brekelmans. "Multi-scale constitutive modelling of heterogeneous materials with a gradient-enhanced computational homogenization scheme". In: *Int. J. Numer. Meth. Engng.* 54.8 (2002), pp. 1235–1260.

[27] R. S. Lakes. "Experimental microelasticity of two porous solids". In: *Int. J. Solids. Struct.* 22.1 (1986), pp. 55–63.

[28] R. S. Lakes. "Size effects and micromechanics of a porous solid". In: *J. Mater. Sci.* 18.9 (1983), pp. 2572–2580.

[29] H.-B. Mühlhaus. "Application of Cosserat theory in numerical solutions of limit load problems". In: *Ingenieur-Archiv* 59.2 (1989), pp. 124–137.

[30] H. C. Park and R. S. Lakes. "Torsion of a micropolar elastic prism of square cross-section". In: *Int. J. Solids. Struct.* 23.4 (1987), pp. 485–503.

[31] G. V. K. Reddy and N. K. Venkatasubramanian. "On the Flexural Rigidity of a Micropolar Elastic Circular Cylinder". In: *J. Appl. Mech.* 45.2 (1978), pp. 429–431.

[32] A. Taliercio. "Torsion of micropolar hollow circular cylinders". In: *Mech. Res. Commun.* 37.4 (2010), pp. 406–411.

[33] C. Tekoğlu et al. "Size effects in foams: Experiments and modeling". In: *Prog. Mater. Sci.* 56.2 (2011), pp. 109–138.

[34] M. A. Wheel, J. C. Frame, and P. E. Riches. "Is smaller always stiffer? On size effects in supposedly generalised continua". In: *Int. J. Solids. Struct.* 67-68 (2015), pp. 84–92.

[35] L. Zybell, U. Mühlich, and M. Kuna. "Constitutive equations for porous plane-strain gradient elasticity obtained by homogenization". In: *Arch. Appl. Mech.* 79.4 (2009), pp. 359–375.